Reconstitution of anaphase DNA bridge recognition and disjunction

Sarlós, Kata; Biebricher, Andreas S.; Bizard, Anna H.; Bakx, Julia A.M.; Ferreté-Bonastre, Anna G.; Modesti, Mauro; Paramasivam, Manikandan; Yao, Qi; Peterman, Erwin J.G.; Wuite, Gijs J.L.; Hickson, Ian D.

published in
Nature Structural and Molecular Biology
2018

DOI (link to publisher)
10.1038/s41594-018-0123-8

document version
Publisher's PDF, also known as Version of record

ARTICLES
https://doi.org/10.1038/s41594-018-0123-8
nature structural & molecular biology

Reconstitution of anaphase DNA bridge recognition and disjunction

Kata Sarlós[1,4], Andreas S. Biebricher[2,4], Anna H. Bizard[1], Julia A. M. Bakx[2], Anna G. Ferreté-Bonastre[1], Mauro Modesti[3], Manikandan Paramasivam[1], Qi Yao[1], Erwin J. G. Peterman[2], Gijs J. L. Wuite[2*] and Ian D. Hickson[1*]

Faithful chromosome segregation requires that the sister chromatids be disjoined completely. Defective disjunction can lead to the persistence of histone-free threads of DNA known as ultra-fine bridges (UFBs) that connect the separating sister DNA molecules during anaphase. UFBs arise at specific genomic loci and can only be visualized by detection of associated proteins such as PICH, BLM, topoisomerase IIIα, and RPA. However, it remains unknown how these proteins work together to promote UFB processing. We used a combination of ensemble biochemistry and new single-molecule assays to reconstitute key steps of UFB recognition and processing by these human proteins in vitro. We discovered characteristic patterns of hierarchical recruitment and coordinated biochemical activities that were specific for DNA structures modeling UFBs arising at either centromeres or common fragile sites. Our results describe a mechanistic model for how unresolved DNA replication structures are processed by DNA-structure-specific binding factors in mitosis to prevent pathological chromosome nondisjunction.

Aneuploidy driven by chromosome missegregation is a feature of many solid tumors[1] and is a driver of maternal-age-associated birth defects[2]. One of the challenges to faithful chromosome segregation is the persistence of DNA interlinks generated during S phase that subsequently prevent timely disjunction of the sister chromatids during anaphase[3]. These DNA interlinks arise principally at specific genomic loci, including centromeres and the ribosomal DNA (rDNA) cluster, telomeres and common fragile sites (CFSs). CFSs are difficult-to-replicate regions that form detectable gaps or breaks on metaphase chromosomes[4] and are hotspots for chromosomal rearrangements in cancer cells[5]. Unresolved DNA interlinks that persist into anaphase generate DNA structures called UFBs[6–8]. Although present in essentially every anaphase, UFBs have remained undetected for decades as a result of being both histone-free and refractory to staining with commonly used dyes such as DAPI. Currently, the only method for visualization of UFBs is via immunofluorescence detection of associated proteins.

Most UFBs are decorated along their length by the SNF2 family translocase PICH, as well as a complex of DNA repair proteins comprising the Bloom's syndrome gene product, BLM, and its partner proteins topoisomerase IIIα (TopoIIIα), RMI1, and RMI2 (denoted henceforth as the BTRR complex)[7,8]. Bloom's syndrome is a rare disorder associated with pre- and postnatal growth retardation, skin abnormalities, and an increase in the incidence of cancer[9,10]. BLM is a RecQ family DNA helicase that has a central role in the BTRR complex in disjoining complex structures that arise during homologous recombination, such as double Holliday junctions[11,12]. Recently, it was demonstrated that mutations in TopoIIIα and RMI1 are present in individuals displaying a Bloom's-like disorder[13]. TopoIIIα is a so-called type 1A topoisomerase that displays only a weak relaxation activity on negatively supercoiled DNA but is efficient as a single-stranded DNA (ssDNA) decatenase[14,15]. RMI1 and RMI2 are oligosaccharide/oligonucleotide binding (OB)-fold-containing proteins that apparently lack catalytic activity and instead function as cofactors in the TopoIIIα catalytic cycle[16–19]. As with all topoisomerases, TopoIIIα generates transient breaks in DNA (ssDNA in this case) and passes a second DNA strand through the break. As a part of this catalytic cycle, TopoIIIα binds covalently to the 5′ end of the broken DNA strand[20].

It is generally accepted that at least three structurally distinct classes of UFBs exist. This assertion is based on two observations. The first is that the frequency of UFB formation at different loci can be modulated by treatment of cells with different chemical agents. Interference with sister chromatid disjunction in mitosis using the TopoIIα inhibitor ICRF-193 leads to the persistence of both centromeric and rDNA-derived UFBs, which is exacerbated in cells lacking PICH[8,21,22]. In contrast, slowing of the DNA replication program using the replicative polymerase inhibitor aphidicolin induces the formation of CFSs and telomeric UFBs[23–25]. These observations argue that ICRF-193-induced UFBs comprise fully replicated, but catenated, DNA, whereas the aphidicolin-induced UFBs comprise incompletely replicated DNA[6]. Regardless of their origin, PICH and the BTRR complex associate with both of these forms of UFB, which are generally considered to comprise largely double-stranded DNA (dsDNA). PICH has a high affinity for dsDNA[26] and acts as a recruitment platform for the other UFB-binding factors[8]. Thus, in PICH-deficient cells, the BTRR complex fails to localize to UFBs, leading to defective UFB processing[8]. Consistent with this, UFBs can persist beyond anaphase in Bloom's syndrome cells[8].

The second observation that revealed the presence of a distinct class of UFBs was that, following perturbation of homologous recombination repair, UFBs arise that are apparently composed mainly of ssDNA[27]. These UFBs, which are not known to arise at any specific locus, are coated with replication protein A (RPA), the

[1]Center for Chromosome Stability and Center for Healthy Aging, Department of Cellular and Molecular Medicine, University of Copenhagen, Copenhagen, Denmark. [2]Department of Physics and Astronomy and LaserLaB, Vrije Universiteit Amsterdam, Amsterdam, The Netherlands. [3]Cancer Research Center of Marseille, CNRS UMR7258, INSERM U1068, Institut Paoli-Calmettes, Aix-Marseille Université UM105, Marseille, France. [4]These authors contributed equally: Kata Sarlós, Andreas S. Biebricher. *e-mail: g.j.l.wuite@vu.nl; iandh@sund.ku.dk

major ssDNA-binding factor in human cells. PICH and RPA occasionally associate with the same UFB, but their patterns of localization are generally non-overlapping in those cases[28,29]. This is consistent with PICH being a dsDNA-specific binding protein.

We reconstituted the recognition and processing of two of the main classes of UFBs: centromeric UFBs (cUFBs) and CFS-associated UFBs (fsUFBs). Using a combination of ensemble biochemistry on DNA substrates mimicking the catenated regions of cUFBs and fsUFBs, with single-molecule optical tweezer assays to define how PICH, RPA, and BTRR complexes associate with different DNA structures, we found that PICH provides a landing pad to alter the binding specificity of BTRR. Moreover, we found that RPA excludes BTRR from ssDNA and prevents any nonspecific cleavage of ssDNA by TopoIIIα, which would have disastrous consequences if it were to occur in anaphase. Our data enhance understanding of how 'problematic' genomic loci are segregated during cell division and provide a methodological approach for analyzing the roles of other genome stability factors at these loci.

Results

A toolkit for reconstitution of UFB processing in vitro. Although the architecture of the DNA in each class of UFBs can be predicted from the types of perturbation that induce their formation, the role of each UFB-associated protein in facilitating sister chromatid disjunction is still debated. To better understand the physiology of UFB processing, we purified fluorescently labeled versions of PICH, BLM, the TRR complex, and RPA (Supplementary Fig. 1a). We then analyzed their DNA-binding properties using dual-trap optical tweezers combined with multicolor fluorescence microscopy (Fig. 1a). In this assay, a 49-kb phage λ dsDNA molecule with biotinylated termini was attached to streptavidin-coated microspheres that were held by optical traps generated by a near-infrared laser. The microspheres were manipulated in a specifically designed multichannel flow cell, permitting the DNA construct to be exposed sequentially to multiple different proteins[30], each located in a separate channel (Fig. 1b,c). This approach allowed us to develop complex, multistep incubation protocols that can reveal the hierarchical assembly of proteins on model DNA substrates (Fig. 1c–e). Furthermore, the setup permitted the simultaneous imaging of three different protein labels with single-molecule (SM) sensitivity[26,31–33], as confirmed by the observed single-step bleaching events (Supplementary Fig. 1b–d). This also permitted an estimation of the number of bound proteins on each substrate (Supplementary Note 2 and Supplementary Table 1). To be able to determine the interactions of four different proteins, we typically use a combination of three differentially labeled proteins together with one unlabeled protein. For all of the analyses reported here, however, we conducted control measurements using a different combination of labeled and unlabeled proteins. Moreover, we reconstituted the recognition and disjunction of the two major types of UFBs—cUFBs generated by inhibition of dsDNA decatenation and fsUFBs generated by perturbation of DNA replication—as these are predicted to be structurally distinct. Thus, where required, one of the flow channels was also used to generate a tract of ssDNA in a controlled manner, using the exonuclease activity of T7 DNA polymerase (Fig. 1d,e and Supplementary Fig. 1e)[34].

We first validated the expected binding patterns of BLM and TRR on dsDNA and partial ssDNA and dsDNA (Supplementary Fig. 1f–i). As expected, both BLM and TRR had high affinity for ssDNA and negligible affinity for dsDNA. This binding pattern also was not affected by changing the applied force (Supplementary Fig. 1j,k). Thus, we conducted subsequent experiments at a force that was optimal for PICH DNA binding and imaging (25 pN)[26].

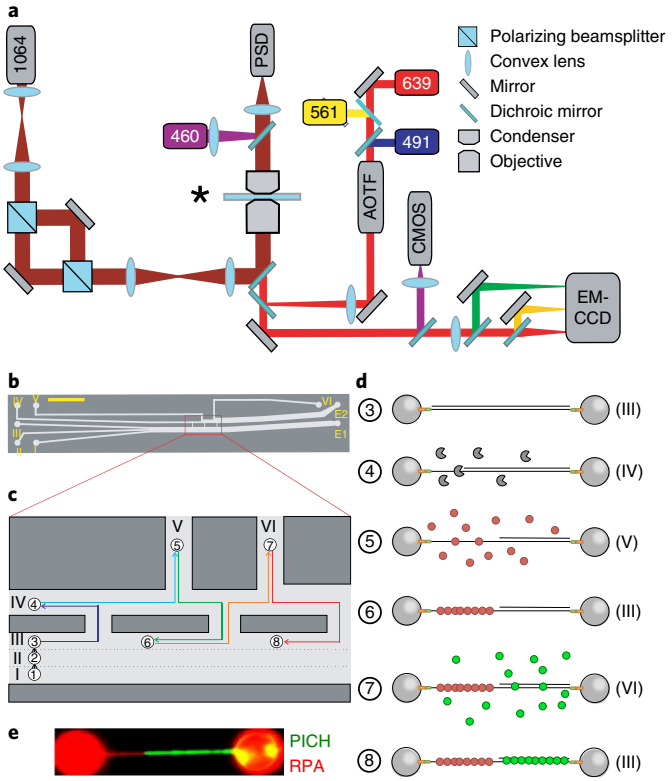

Fig. 1 | Modeling UFBs using optical tweezers combined with fluorescence imaging. a, Experimental setup showing beam paths and crucial components. Dark red lines (left) indicate the infrared laser beam path used to create double optical tweezers and measure applied forces. Light-red-colored lines depict beam paths for bright-field illumination as well as fluorescence excitation and detection. The asterisk indicates the position of the flow cell shown below; a detailed description of the setup is provided in the Methods. 1064, 10-W IR CW laser; 460, LED used for bright-field illumination; PSD, position-sensitive diode; 491, 561, and 639, lasers used for fluorescence excitation; AOTF, acousto-optical tuneable filter; CMOS, CMOS camera for bright-field detection; EIS, emission image splitter; EM-CCD, EM-CCD camera for fluorescence detection. **b**, Scheme of the glass chip used in the SM setup. The chip comprises six inlet channels, I–VI, and two outlet channels, E1 and E2. The yellow scale bar represents 1 cm. **c**, Scheme of the central portion of the glass chip displaying the connections between the six channels used for DNA capture and protein incubation. Arabic numbers denote the steps needed to conduct a typical SM experiment; arrows indicate the translocation paths. A typical example is shown in which beads (I) and DNA (II) are captured, stretched in buffer (III), and subsequently incubated in the protein channels containing T7 polymerase (IV), RPA (V), and PICH (VI). **d**, Schematic diagram of the DNA held by beads and the binding of proteins induced during experimental steps 1–8 displayed in **b**. Roman numbers in brackets indicate the channel in which the incubation occurred; Arabic numbers refer to the sequential course of the experiment as shown in **c**. 1, beads are trapped in channel I; 2, DNA is captured in channel II; 3, a single dsDNA molecule is tethered between the beads in channel III; 4, the exonuclease activity of T7 polymerase in channel IV is used to create a partial ssDNA or dsDNA molecule; 5, the construct is incubated in RPA in channel V; 6, RPA coating is visualized by imaging in a protein-free environment (channel III); 7, the construct is incubated with PICH in channel VI; 8, a final fluorescence snapshot in channel III is made to display the spatial localization of bound proteins. **e**, Typical dual-color fluorescence snapshot of RPA^{Strawberry} (red) and PICH^{GFP} (green) resulting after step 8 shown in **c** and **d**.

Reconstitution of protein recruitment to a model of a centromeric UFB. cUFBs can be induced by ICRF-193 (Fig. 2a and Supplementary Fig. 2a)[7,8]. Because the target for ICRF-193 (TopoIIα) is a dsDNA decatenase and cUFBs lack RPA, these structures are considered to be composed of fully replicated, but interlinked, dsDNA. Thus, to investigate potential ways in which cUFBs

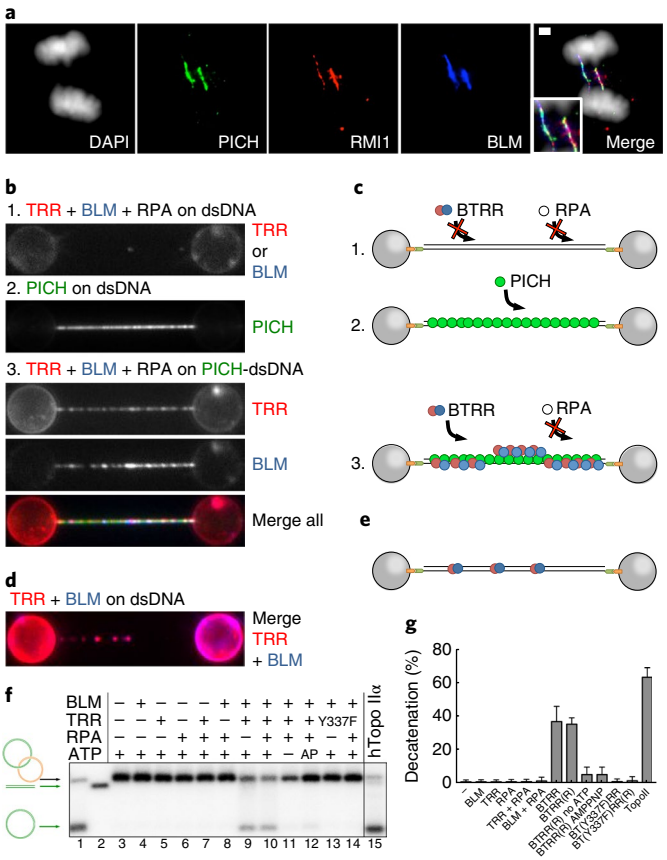

Fig. 2 | Processing of centromeric UFBs by the PICH–BTRR machinery. a, Immunofluorescence images of anaphase U2OS cells treated with ICRF-193 and displaying UFBs coated with PICH (green), TRR (RMI1; red), and BLM (blue). Scale bar, 1 µm. **b**, Use of optical tweezers to model the recruitment of BLM^{SNAP} (labeled with a far-red dye), TRR^{Cherry}, and RPA (unlabeled) to a double-stranded model of a cUFB before (1) and after (3) decorating it with PICH^{GFP} (2). **c**, Schematic representation of the data presented in **b** (blue, BLM; red, TRR; white, RPA; green, PICH). **d**, Fluorescence snapshots of the recruitment of BLM^{SNAP} and TRR^{Cherry} to naked dsDNA in the absence of RPA using optical tweezers. **e**, Schematic representation of the data in **d** (blue, BLM; red, TRR). **f**, Southern blot of an agarose gel showing decatenation of the single-catenane substrate by the BTRR complex with or without RPA (lanes 9 and 10). Lanes 1 and 2 contain the markers for the circular covalently closed and linear products, respectively; lane 3 contains the substrate alone; and lanes 4–8 contain control reactions, where either BLM or TRR is missing. AP denotes AMP-PNP, a non-hydrolyzable ATP analog; Y337F denotes a catalytically dead TRR complex mutant. TopoIIα is shown for comparison (lane 15). Note that the probe allows visualization of one of the circular DNA molecules (green). Reactions contained 5 nM BLM, 1.25 nM TRR or TRR^{Y337F}, 5 nM RPA, and 30 pM TopoIIα. Uncropped gel images are shown in Supplementary Dataset 1. **g**, Quantification of the data from **f** combined with additional experiments. Data shown are means and s.e.m. of $n = 3$ independent experiments. Source data are available online.

might be processed in vitro, we examined protein interactions with dsDNA using our SM assays (Fig. 2b,c and Supplementary Fig. 2b,c). We observed that BTRR was recruited much more efficiently (by more than two orders of magnitude) to PICH-coated dsDNA than to naked dsDNA (Supplementary Table 1). This explains how BTRR appears on the double-stranded cUFBs in cells, despite the known preference of both BLM and TRR for binding ssDNA (Supplementary Fig. 1f–i)[14,35].

RPA forms a complex with BTRR by binding independently to both BLM and RMI1, and is able to modulate the helicase and topoisomerase activities of BTRR in vitro[36,37]. However, RPA did not readily associate with BTRR that was recruited to PICH-coated DNA (Supplementary Fig. 2b,c), which is consistent with the observation that RPA does not generally localize to PICH-coated UFB tracts in vivo[28]. Nevertheless, we observed that RPA reduced the modest nonspecific binding of BTRR to naked dsDNA, which is consistent with the observation that these proteins form a complex in solution (Fig. 2b,d and Supplementary Table 1). It should be noted that the association of BTRR with naked dsDNA even in the absence of RPA is still much lower than its association with PICH-coated dsDNA (Supplementary Table 1). However, because RPA is an abundant cellular protein and a proportion of the RPA pool appears to be constitutively associated with the BTRR complex[17], we conducted experiments in the presence of RPA, as these better reflect the physiological situation.

An important feature of our flow chamber was that, by keeping PICH and BTRR–RPA in separate channels, we could investigate the recruitment of the BTRR complex to naked versus PICH-coated dsDNA using the same DNA molecule (before or after PICH incubation). Nevertheless, we confirmed in control experiments containing all four proteins in the same channel that preincubation of PICH and BTRR did not considerably alter their DNA-binding and recruitment properties (Supplementary Fig. 2d,e and Supplementary Table 1).

The BTRR complex can disjoin a cUFB-like DNA substrate. Although direct recruitment by PICH explains how the BTRR complex recognizes double-stranded cUFBs, it does not address the mechanism of cUFB processing. To this end, we used ensemble biochemistry to study a single-catenane substrate comprising two interlinked, supercoiled dsDNA plasmids (Supplementary Fig. 3a,b)[38]. We observed that BTRR could decatenate this substrate into its constituent plasmids, albeit with a much lower efficiency than TopoIIα, the only known dsDNA decatenase to act on cUFBs (Fig. 2f,g). This dsDNA decatenase activity of the BTRR complex appears to be evolutionarily conserved, as a similar activity has also been observed with the bacterial and yeast orthologs of these proteins[39,40]. Notably, the previously described activities were highly dependent on the presence of a ssDNA-binding protein, whereas RPA had no substantial effect on this reaction in our case, which is consistent with our SM analysis (Supplementary Fig. 2b,c). Similarly, PICH did not alter the efficiency of the dsDNA decatenase activity of BTRR (Supplementary Fig. 3b–d), suggesting that PICH acts primarily to increase the local concentration of the BTRR complex on cUFBs in vivo.

BLM and TRR can be recruited independently to PICH-coated UFBs. BTRR was present as a complex on PICH-coated dsDNA and on naked dsDNA, as shown by colocalization of the fluorescence intensity profiles of BLM and TRR under both high- and low-DNA-coating conditions (Supplementary Fig. 4a–d). We investigated the mechanism by which BTRR was recruited to PICH-coated UFBs in vivo using cell lines lacking either BLM (Bloom's syndrome cells; PSNG13)[41] or TopoIIIα. Because TopoIIIα is essential for viability, we used an HCT116 cell derivative in which TopoIIIα could be depleted at the G2/M boundary through an auxin-based degron system[42]. Using these cell lines, we observed that TopoIIIα localized to PICH-coated UFBs in the Bloom's syndrome cell line and that BLM associated with UFBs in TopoIIIα-depleted cells when both TopoIIIα and RMI1 were absent from these UFBs (Fig. 3a–c and Supplementary Fig. 4e–g). Consistent with these observations, BLM and TRR were able to independently bind to PICH-coated dsDNA in our SM assays (Fig. 3d–f). However, BTRR as a complex showed a higher affinity for PICH-coated dsDNA than did BLM or TRR alone (Fig. 3g and Supplementary Table 1), suggesting that BTRR is likely to be recruited in vivo as a complex to PICH-coated UFBs.

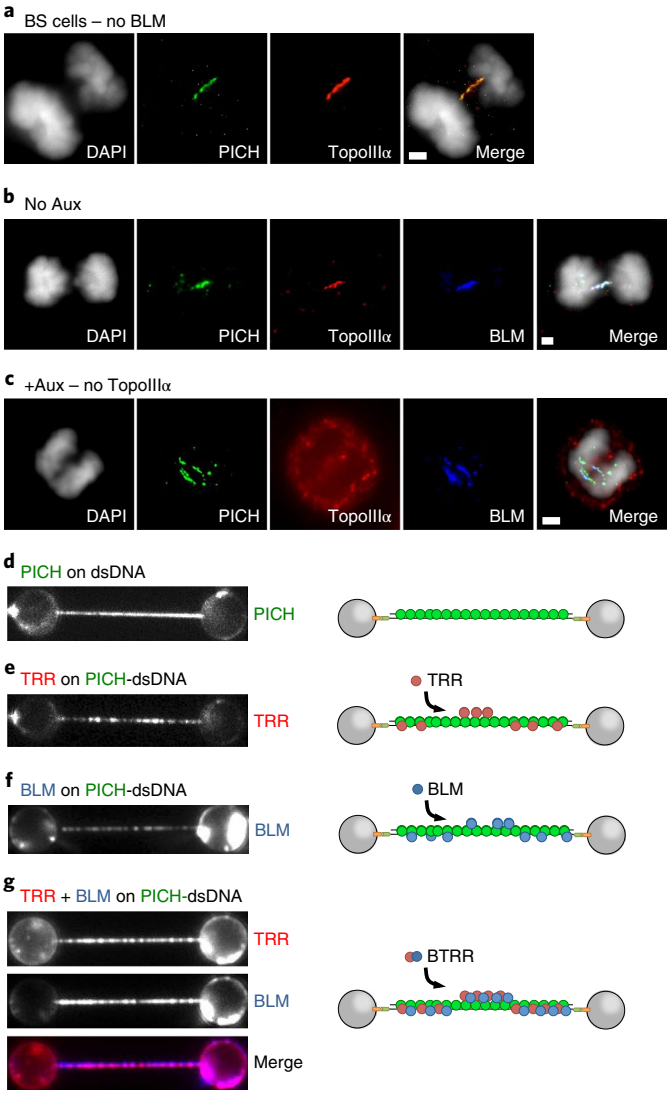

Fig. 3 | PICH recruits BLM and TRR independently to dsDNA. a, Immunofluorescence image of a UFB coated by PICH (green) and TRR (red) in a Bloom's syndrome (BS) cell line (PSNG13). Scale bar, 2 µm. **b**, Immunofluorescence image of a UFB coated by PICH (green), TopoIIIα (red), and BLM (blue) in an HCT116 cell line in which TopoIIIα was not degraded. Scale bar, 1 µm. **c**, Immunofluorescence image of a TopoIIIα-negative (red) UFB coated by PICH (green) and BLM (blue) in an HCT116 cell line in which TopoIIIα was degraded before mitosis. Scale bar, 1 µm. **d**, Fluorescence snapshots (left) and schematic representation (right) of the recruitment of $PICH^{GFP}$ (green) to a model of a UFB using optical tweezers. **e**, Fluorescence snapshots (left) and schematic representation (right) of the recruitment of TRR^{Cherry} (red) to a $PICH^{GFP}$-coated (green) model of a UFB using optical tweezers. **f**, Fluorescence snapshots (left) and schematic representation (right) of the recruitment of BLM^{SNAP} (blue) to a $PICH^{GFP}$-coated (green) model of a UFB using optical tweezers. **g**, Fluorescence snapshots (left) and schematic representation (right) of the recruitment of BTRR (BLM^{SNAP}, blue; TRR^{Cherry}, red) to a $PICH^{GFP}$-coated (green) model of a UFB using optical tweezers.

The catalytic activity of PICH is not required for BTRR recruitment to UFBs. Because PICH can translocate along dsDNA using the energy of ATP hydrolysis[26], we investigated whether PICH might also modify the structure of the dsDNA to make it permissive for BTRR binding. To achieve this, we analyzed both in vivo and in vitro the recruitment of BTRR to dsDNA decorated by a variant

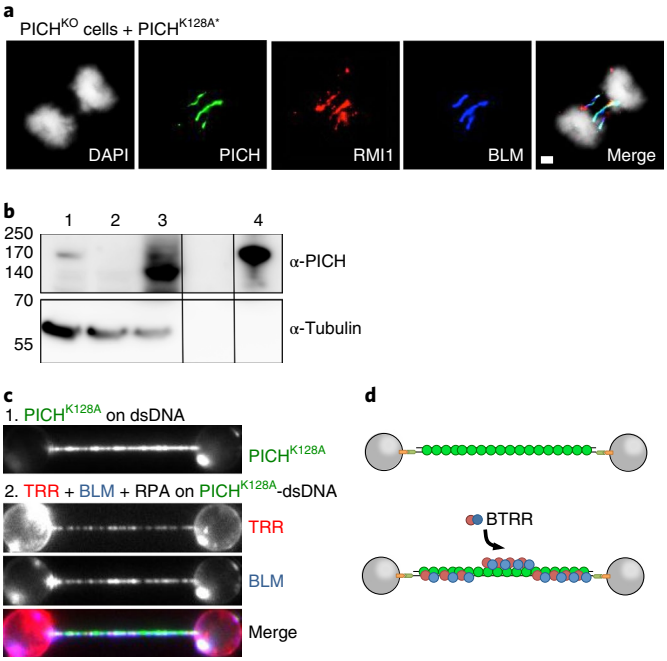

Fig. 4 | PICH activity is not required for BTRR recruitment. a, Immunofluorescence images of a UFB induced by ICRF-193 in a PICH-knockout (KO) HT1080 cell line complemented by the catalytically dead $PICH^{K128A}$ protein (green, PICH; red, TRR; blue, BLM). Scale bar, 1 µm. **b**, Western blot analysis of the PICH-knockout HT1080 cell line and the reconstitution of these cells using $PICH^{K128A\text{-}GFP}$. Lanes: 1, PICH-knockout cells complemented with $PICH^{K128A\text{-}GFP}$; 2, PICH knockout; 3, HT1080 wild type; 4, purified recombinant $PICH^{GFP}$. Uncropped blot images are shown in Supplementary Dataset 1. **c**, Modeling the recruitment to a $PICH^{K128A\text{-}GFP}$-coated dsDNA (1) of BLM^{SNAP}, TRR^{Cherry}, and RPA (unlabeled) (2) using optical tweezers. **d**, Schematic representation of the data from **b** (blue, BLM; red, TRR; green, PICH).

of PICH ($PICH^{K128A}$) that still binds dsDNA but lacks ATPase and translocase activity. We observed that BTRR was proficient in binding to cUFBs in a PICH-knockout cell line expressing the $PICH^{K128A}$ protein (Fig. 4a,b). Furthermore, BLM and TRR were each able to bind to $PICH^{K128A}$-coated dsDNA in vitro (Fig. 4c,d). These data indicate that the catalytic activity of PICH does not facilitate the binding of BTRR to UFBs. Taking these data together, we propose that PICH nucleates the BTRR complex onto cUFBs to promote the timely resolution of interlinked dsDNA catenanes during anaphase, when TopoIIα activity is limiting or ineffective.

Reconstitution of protein recruitment to CFS UFBs. Next, we compared the activity of the PICH, RPA, and BTRR proteins on a model substrate that mimics an fsUFB. In contrast to cUFBs, fsUFBs (Supplementary Fig. 5a) often contained some ssDNA as well as dsDNA, as revealed by combined but generally non-overlapping staining for RPA and PICH (Fig. 5a). The BTRR complex was also detectable on fsUFBs but only on the PICH-coated dsDNA regions. This was surprising to us given that BLM and TRR each bind with high affinity to ssDNA and that RPA interacts directly with both BLM and RMI1[14,17,35,37]. In SM experiments, when a partial ssDNA and dsDNA substrate (Fig. 5b,c and Supplementary Fig. 5b,c) was incubated with a mixture of BLM, TRR, and RPA, we observed that the single-stranded section was coated with RPA but not with BLM or TRR (Fig. 5b and Supplementary Fig. 1g–i). In contrast, when RPA was omitted, the ssDNA portion was strongly coated with BLM and TRR (Supplementary Fig. 5d,e). These results indicate that RPA is responsible for exclusion of the BTRR complex from ssDNA,

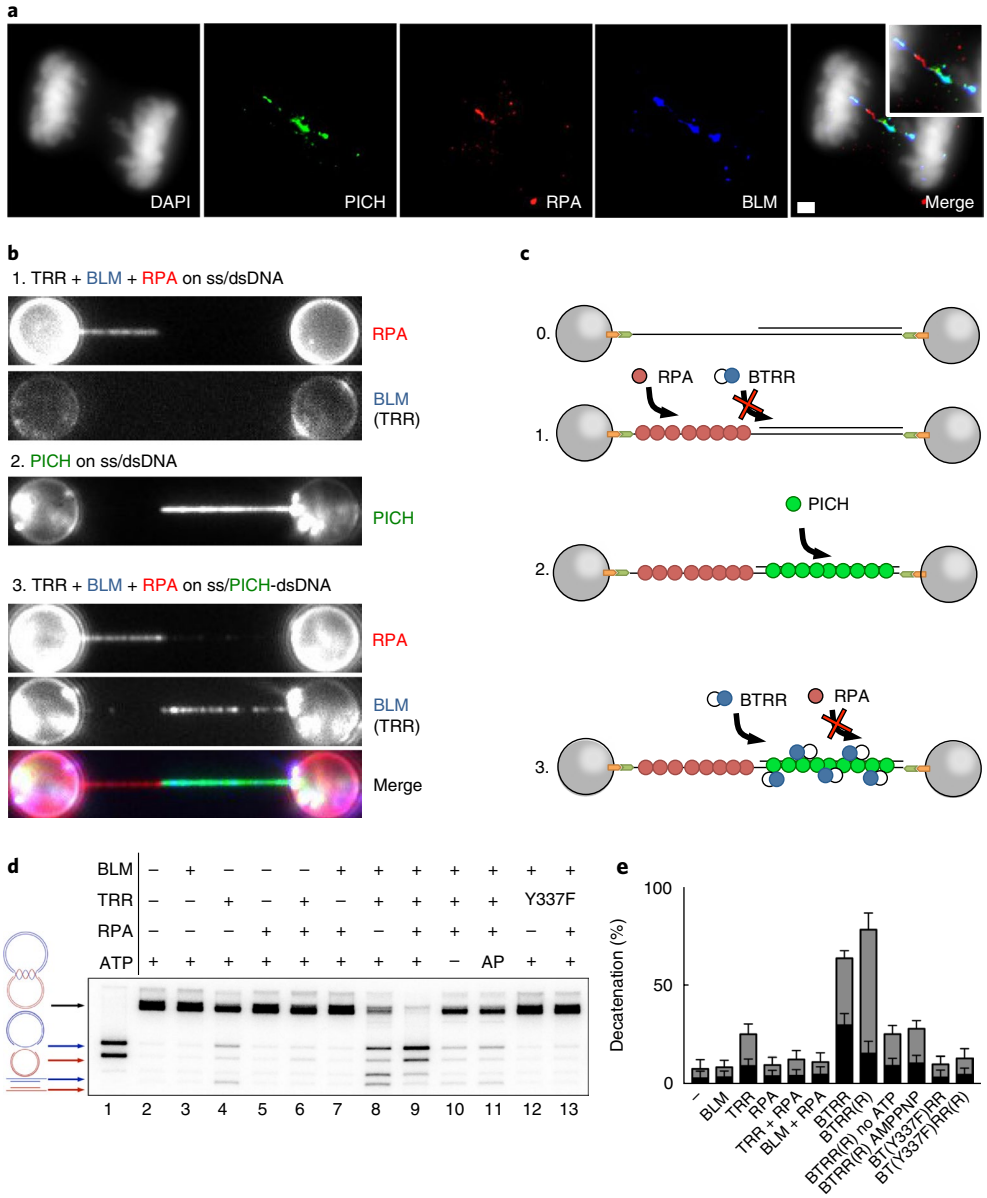

Fig. 5 | Processing of fragile-site UFBs by the PICH–BTRR machinery. a, Immunofluorescence images of anaphase U2OS cells treated with aphidicolin and displaying UFBs coated with PICH (green), RPA (red), and BLM (blue). Scale bar, 1 μm. **b**, Use of optical tweezers to model the recruitment of BLM^{SNAP}, TRR (not labeled), and $RPA^{Strawberry}$ to a partial single- and double-stranded model of an fsUFB before (1) and after (3) decorating it with $PICH^{GFP}$ (2). **c**, Schematic representation of the naked ssDNA and dsDNA (0) and the DNA-bound proteins (1–3) presented in **b** (blue, BLM; white, TRR; red, RPA; green, PICH). **d**, Agarose gel showing disjunction of the LRI substrate by the BTRR complex with or without RPA (lanes 8 and 9). Lane 1 contains the markers for the circular products; lane 2 contains the substrate alone; and lanes 3–7 contain control reactions, where either BLM or TRR is missing. AP denotes AMP-PNP, a non-hydrolyzable ATP analog; Y337F denotes a catalytically dead TRR complex mutant. Reactions contained 20 nM BLM, 5 nM TRR or TRR^{Y337F}, and 30 nM RPA. Uncropped gel images are shown in Supplementary Dataset 1. **e**, Quantification of the combined data from **d** and additional experiments (gray bars, circular DNA products; black bars, linear DNA products). Data shown are means and s.e.m. from $n = 6$ independent experiments. Source data are available online.

thereby markedly reducing the amount of BTRR on ssDNA by more than two orders of magnitude (Supplementary Table 1).

The BTRR complex can disjoin an fsUFB-like DNA substrate. Given that CFSs are particularly susceptible to DNA replication stress and have been shown to be among the final regions of the genome to be replicated[43], it is highly likely that fsUFBs comprise a form of DNA replication intermediate in which the merging of converging forks has been delayed. To study the action of the BTRR complex on fsUFBs, we created a substrate mimicking an incompletely replicated DNA molecule. This late-replication intermediate (LRI) structure was composed of two interlinked DNA circles containing a region resembling two converging replication forks (Supplementary Fig. 6). We observed that BTRR could catalyze LRI disjunction (Fig. 5d,e) with comparable kinetics to that of another well-characterized biochemical activity of the BTRR complex, double–Holliday junction dissolution[11] (Supplementary Fig. 7a–c). This activity of the BTRR also seems to be evolutionarily conserved, as the bacterial homologs could also disjoin a similar substrate[44]. Moreover, PICH modestly stimulated this reaction in an ATP-dependent

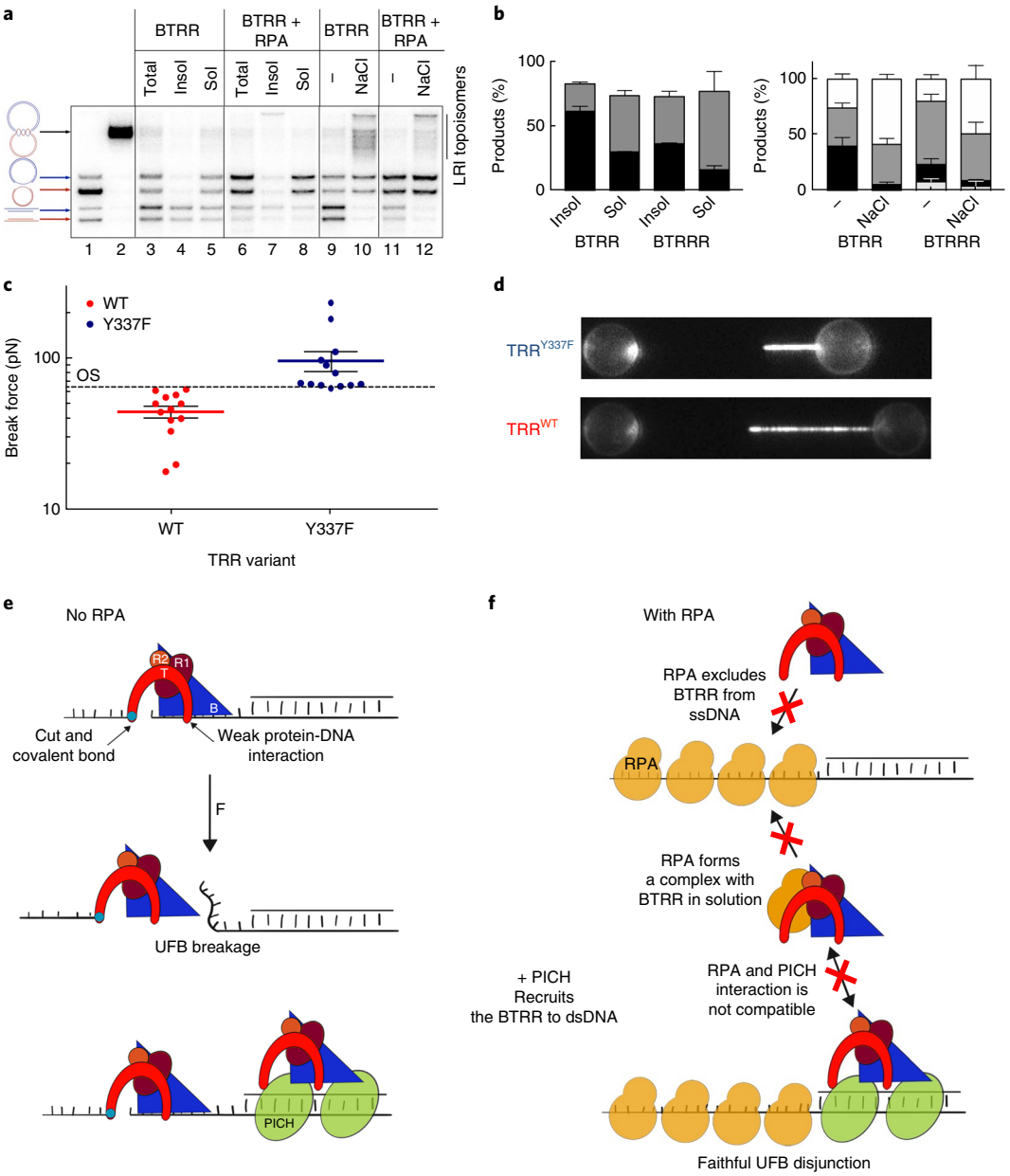

Fig. 6 | RPA excludes the BTRR complex from ssDNA to prevent nonspecific breakage of UFBs. a, Agarose gel showing disjunction of the LRI substrate by the BTRR and RPA complex. Lane 1 contains the circular and linear product markers; lane 2 contains the substrate only. In lanes 3, 6, 9, and 11, the reactions were terminated as normal with EDTA. In lanes 4, 5, 7, and 8, the reactions were terminated using the SDS-KCl method. In lanes 10 and 12, the reactions were stopped by the addition of 500 mM NaCl. Reactions contained 20 nM BLM, 5 nM TRR, and 30 nM RPA. Uncropped gel images are shown in Supplementary Dataset 1. **b**, Quantification of the data from **a** combined with additional experiments (white bars, LRI; dark gray bars, circular DNA; black bars, linear DNA; light gray bars, ssDNA). Data shown are means and s.e.m. from $n=3$ independent experiments. **c**, Distribution of the forces required to break a partial ssDNA or dsDNA molecule coated with either $TRR^{WT\text{-}Cherry}$ (red) or $TRR^{Y337F\text{-}Cherry}$ (blue). The force required to overstretch (OS) DNA (at which point dsDNA is converted to ssDNA) is marked by a horizontal dashed line. Data shown are means and s.e.m. from $n=13$ measurements. Source data are available online. **d**, Representative fluorescence snapshots from the optical tweezers of either $TRR^{Y337F\text{-}Cherry}$ (top) or $TRR^{WT\text{-}Cherry}$ (bottom) coating the ssDNA part of a DNA molecule held with a force of 25 pN. Note that both images contain a similar amount of ssDNA; however, in the case of $TRR^{WT\text{-}Cherry}$, the ssDNA has a higher degree of extension. **e**,**f**, Schematic representation of the action of the BTRR complex on DNA in the absence (**e**) and presence (**f**) of RPA or PICH. (F denotes force applied to the UFB by the mitotic spindle; green, PICH; yellow, RPA; blue triangle, BLM; red arch, TopoIII; dark red and orange circles marked R1 and R2, RMI1/2.)

manner (Supplementary Fig. 7d,e). These data indicate that PICH likely has a dual role at fsUFBs in both protein recruitment and stimulation of the BTRR complex in vivo.

RPA protects single-stranded UFBs from unscheduled breakage by TRR. Analysis of the products of the LRI disjunction reaction revealed that, in addition to the expected gapped circular products formed by the cleavage/re-ligation cycle of TopoIIIα, two additional linear molecules were formed. Inclusion of RPA not only enhanced the efficiency of the LRI disjunction reaction, but also largely prevented the accumulation of these linear products (Fig. 5d). The catalytic cycle of type IA topoisomerases requires a transesterification

reaction to create a covalent intermediate between the 5′ end of the DNA and the active site tyrosine of the topoisomerase. The 3′ end of the cleaved DNA is bound via a noncovalent interaction. After strand passage, the broken DNA ends are then resealed by the topoisomerase[20]. We hypothesized that the linear products forming in the absence of RPA might represent the normally transient cleaved intermediate where TopoIIIα has failed to re-ligate the DNA. If that were the case, the enzyme would remain covalently attached to the 5′ end of the DNA but would then be removed during the deproteinization step of the reaction to reveal the broken DNA. To investigate this, we omitted deproteinization and instead precipitated the proteins at the end of the reaction using SDS-KCl, which is a standard method to confirm covalent attachment between topoisomerases and DNA[45]. Indeed, the precipitated (insoluble) fraction contained the cleaved linear DNA fragments, confirming that they were covalently bound to TopoIIIα (Fig. 6a,b). Furthermore, addition of high salt at the end of the incubation period, which enforces closure of the broken DNA ends by type IA topoisomerases while preventing initiation of a new catalytic cycle[46], resulted in re-closure of all of the cleaved products, appearing as a spectrum of interlinked LRIs (Fig. 6a).

Notably, neither a DNA-binding-deficient form of RPA nor *Escherichia coli* SSB (the prokaryotic homolog of RPA) could stimulate LRI disjunction or promote the re-ligation of cut DNA by TopoIIIα (Supplementary Fig. 8). This indicates that RPA has to bind to ssDNA as well as to associate with BTRR to simultaneously limit the formation of unligated products and promote LRI disjunction.

To model the proposed unimpeded cleavage of naked (RPA-free) ssDNA by TRR in mitosis, we compared the force required to break a partial ssDNA or dsDNA molecule in which the ssDNA portion was coated by either wild-type TRR (TRR^{WT}) or a catalytically inactive mutant TRR (TRR^{Y337F}) to control for the presence of any contaminating nucleases. We observed that ssDNA coated by TRR^{WT} broke at forces (45 ± 4 pN, mean and s.e.m. for $n = 13$ measurements) well below the known DNA overstretching transition point[47], whereas ssDNA coated by TRR^{Y337F} required much higher forces (96 ± 14 pN, mean and s.e.m. for $n = 13$ measurements) (Fig. 6c,d). It should be noted that, at such high forces, the DNA associated with TRR^{Y337F} is susceptible to breakage as a result of its intrinsic instability[48]. These observations suggest that, following creation of the covalent cleaved intermediate between TRR^{WT} and DNA, noncovalent association of TopoIIIα with the 3′ end of the cleaved DNA is susceptible to rupture by an applied force of ~45 pN. Furthermore, ssDNA and dsDNA molecules incubated with BTRR and RPA (where RPA largely excludes the BTRR complex from ssDNA) did not show any breakage below overstretching forces (Supplementary Fig. 9a,b). Taken together, these results indicate that uncoupling of the cleavage and re-ligation cycle of TRR would be detrimental if it were to happen on a UFB comprising naked ssDNA (Fig. 6e). This might lead to unscheduled and irreversible UFB breakage as a result of the tension exerted by mitotic spindle forces, which could drive chromosomal abnormalities in the daughter cells. We therefore propose that exclusion of the TRR complex from the ssDNA portion of UFBs by RPA reflects an important physiological mechanism to prevent irreversible chromosome damage (Fig. 6f).

Discussion

Our findings demonstrate how a combination of in vivo and in vitro approaches can be used to gain insight into the recognition and disjunction of UFBs. We have reconstituted anaphase UFB processing at centromeres and CFSs in vitro using two methods: an innovative flow channel system combined with optical trapping and three-color fluorescence imaging, and ensemble biochemistry involving DNA substrates mimicking intermediates in DNA metabolism that are thought to generate UFBs. We suggest that this methodology will be very useful for studying the function of other UFB-binding factors, such as RIF1 and FANCM.

Our in vitro observations explain phenomena observed during direct visualization of UFBs in human cells and are consistent with a model (Supplementary Fig. 10) in which PICH recognizes dsDNA sections of UFBs under tension and recruits the BTRR complex. The vast majority of the UFBs present at CFSs are then resolved by the ssDNA decatenase activity of the BTRR complex in a reaction that is modulated by both PICH and RPA. More specifically, the intricate interplay between BTRR recruitment by PICH and exclusion of BTRR binding to ssDNA by RPA ensures the faithful and timely disjunction of sister chromatids. Moreover, although the vast majority of the dsDNA catenanes remaining in the genome after replication are eliminated by TopoIIα, whose activity is also assisted by PICH[22] before or soon after anaphase onset, we propose that the BTRR complex might serve as a backup system to rescue anaphase in those rare cases in which TopoIIα function is compromised. Because anaphase is such a brief event, we envisage three scenarios in which the proposed BTRR pathway might become critical for chromatid disjunction: first, when a cell enters mitosis with an unusually large number of DNA interlinks (for example, following a perturbed S phase) and TopoIIα is overwhelmed; second, when unresolved DNA interlinks fail to be efficiently detected by TopoIIα during early anaphase (in this regard, TopoIIα is concentrated at centromeres during early anaphase[49], where the bulk of the persistent dsDNA linkages occur, but may be limiting at other loci); and third, when the underlying structure of the interlinked DNA is distorted, perhaps because of the tension applied to the DNA, which has been shown to affect the efficiency of unlinking by TopoIIα[50].

In addition to deciphering the mechanisms of UFB disjunction, our data also reveal how the activity of the BTRR complex is regulated by RPA so as to limit unscheduled ssDNA breakage. We found that RPA, which hitherto has been viewed as a constitutive component of the BLM–TRR complex[51], also acts as a negative regulator of the TRR complex by protecting ssDNA from unscheduled, TopoIIIα-mediated cleavage. Given that BTRR alone displays a high affinity for ssDNA, one possible mechanism would be that, in the ternary protein complex, the ssDNA-binding sites of BTRR are occluded by RPA. Thus, our findings reveal a complex network of interactions among UFB-binding proteins that serve to recognize the presence of a UFB in a markedly short timeframe in early anaphase and then promote timely disjunction of the DNA interlinks.

A new class of mixed ssDNA- and dsDNA-containing UFBs was recently discovered[27]. These UFBs, which arise as a consequence of perturbation of homologous recombination, do not arise from either centromeres or CFSs, and have been proposed to comprise unresolved recombination intermediates (HR-UFBs). It would be of interest in the future to decipher mechanistic differences between the processing of these HR-UFBs and fsUFBs. Given that HR-UFBs were shown to bind BLM, RPA, and PICH, and BTRR and RPA are central players in the processing of homologous recombination intermediates[11,52], it is possible that HR-UFBs will also be processed by the BTRR complex. It has also been proposed that HR-UFBs are processed by the helicase activity of BLM, thereby converting a PICH-coated dsDNA UFB into RPA-coated ssDNA. Given that BLM alone is a weak helicase and only becomes processive when coupled with TRR and RPA[53], such bridge unwinding would likely require BTRR to access the ssDNA and dsDNA junction of a UFB in conjunction with PICH and RPA. This is consistent with our SM recruitment experiments using mixed ssDNA and dsDNA molecules, where we frequently observed that, although BTRR was excluded from ssDNA by RPA, the junction of the ssDNA and dsDNA showed a prominent spot of BTRR. Indeed, it is possible that BTRR gets recruited to the complete length of a PICH-coated UFB yet only initiates a catalytic cycle when it encounters a high-affinity substrate such as would be found at a ssDNA and dsDNA

junction or catenated region. This is also corroborated by the fact that BTRR is only weakly effective in resolving dsDNA catenanes but is very efficient in resolving LRIs in the presence of RPA, a substrate that contains two ssDNA and dsDNA junctions. Given that RPA excludes BTRR from ssDNA sections, this would leave the junction as a major nucleation point for initiation of unwinding and decatenation. Investigating this in the future would be important for obtaining a more complete understanding of the mechanism of UFB disjunction.

Online content

Any methods, additional references, Nature Research reporting summaries, source data, statements of data availability and associated accession codes are available at https://doi.org/10.1038/s41594-018-0123-8.

Received: 15 May 2018; Accepted: 1 August 2018;
Published online: 3 September 2018

References

1. Thompson, S. L. & Compton, D. A. Chromosomes and cancer cells. *Chromosome Res.* **19**, 433–444 (2011).
2. Herbert, M., Kalleas, D., Cooney, D., Lamb, M. & Lister, L. Meiosis and maternal aging: insights from aneuploid oocytes and trisomy births. *Cold Spring Harb. Perspect. Biol.* **7**, a017970 (2015).
3. Mankouri, H. W., Huttner, D. & Hickson, I. D. How unfinished business from S-phase affects mitosis and beyond. *EMBO J.* **32**, 2661–2671 (2013).
4. Durkin, S. G. & Glover, T. W. Chromosome fragile sites. *Annu. Rev. Genet.* **41**, 169–192 (2007).
5. Glover, T. W., Wilson, T. E. & Arlt, M. F. Fragile sites in cancer: more than meets the eye. *Nat. Rev. Cancer* **17**, 489–501 (2017).
6. Sarlós, K., Biebricher, A., Petermann, E. J. G., Wuite, G. J. L. & Hickson, I. D. Knotty problems during mitosis: mechanistic insight into the processing of ultrafine DNA bridges in anaphase. *Cold Spring Harb. Symp. Quant. Biol.* **82**, 187–195 (2017).
7. Baumann, C., Körner, R., Hofmann, K. & Nigg, E. A. PICH, a centromere-associated SNF2 family ATPase, is regulated by Plk1 and required for the spindle checkpoint. *Cell* **128**, 101–114 (2007).
8. Chan, K. L., North, P. S. & Hickson, I. D. BLM is required for faithful chromosome segregation and its localization defines a class of ultrafine anaphase bridges. *EMBO J.* **26**, 3397–3409 (2007).
9. Cunniff, C., Bassetti, J. A. & Ellis, N. A. Bloom's syndrome: clinical spectrum, molecular pathogenesis, and cancer predisposition. *Mol. Syndromol* **8**, 4–23 (2017).
10. German, J., Sanz, M. M., Ciocci, S., Ye, T. Z. & Ellis, N. A. Syndrome-causing mutations of the *BLM* gene in persons in the Bloom's Syndrome Registry. *Hum. Mutat.* **28**, 743–753 (2007).
11. Wu, L. & Hickson, I. D. The Bloom's syndrome helicase suppresses crossing over during homologous recombination. *Nature* **426**, 870–874 (2003).
12. Bachrati, C. Z., Borts, R. H. & Hickson, I. D. Mobile D-loops are a preferred substrate for the Bloom's syndrome helicase. *Nucleic Acids Res.* **34**, 2269–2279 (2006).
13. Martin, C. A. et al. Mutations in *TOP3A* cause a Bloom's syndrome–like disorder. *Am. J. Hum. Genet.* **103**, 221–231 (2018).
14. Goulaouic, H. et al. Purification and characterization of human DNA topoisomerase IIIα. *Nucleic Acids Res.* **27**, 2443–2450 (1999).
15. Yang, J., Bachrati, C. Z., Ou, J., Hickson, I. D. & Brown, G. W. Human topoisomerase IIIα is a single-stranded DNA decatenase that is stimulated by BLM and RMI1. *J. Biol. Chem.* **285**, 21426–21436 (2010).
16. Wu, L. et al. BLAP75/RMI1 promotes the BLM-dependent dissolution of homologous recombination intermediates. *Proc. Natl. Acad. Sci. USA* **103**, 4068–4073 (2006).
17. Xu, D. et al. RMI, a new OB-fold complex essential for Bloom syndrome protein to maintain genome stability. *Genes Dev.* **22**, 2843–2855 (2008).
18. Singh, T. R. et al. BLAP18/RMI2, a novel OB-fold-containing protein, is an essential component of the Bloom helicase–double Holliday junction dissolvasome. *Genes Dev.* **22**, 2856–2868 (2008).
19. Yin, J. et al. BLAP75, an essential component of Bloom's syndrome protein complexes that maintain genome integrity. *EMBO J.* **24**, 1465–1476 (2005).
20. Vos, S. M., Tretter, E. M., Schmidt, B. H. & Berger, J. M. All tangled up: how cells direct, manage and exploit topoisomerase function. *Nat. Rev. Mol. Cell Biol.* **12**, 827–841 (2011).
21. Nielsen, C. F. & Hickson, I. D. PICH promotes mitotic chromosome segregation: identification of a novel role in rDNA disjunction. *Cell Cycle* **15**, 2704–2711 (2016).
22. Nielsen, C. F. et al. PICH promotes sister chromatid disjunction and co-operates with topoisomerase II in mitosis. *Nat. Commun.* **6**, 8962 (2015).
23. Chan, K. L., Palmai-Pallag, T., Ying, S. & Hickson, I. D. Replication stress induces sister-chromatid bridging at fragile site loci in mitosis. *Nat. Cell Biol.* **11**, 753–760 (2009).
24. Barefield, C. & Karlseder, J. The BLM helicase contributes to telomere maintenance through processing of late-replicating intermediate structures. *Nucleic Acids Res.* **40**, 7358–7367 (2012).
25. Burrell, R. A. et al. Replication stress links structural and numerical cancer chromosomal instability. *Nature* **494**, 492–496 (2013).
26. Biebricher, A. et al. PICH: a DNA translocase specially adapted for processing anaphase bridge DNA. *Mol. Cell* **51**, 691–701 (2013).
27. Chan, Y. W., Fugger, K. & West, S. C. Unresolved recombination intermediates lead to ultra-fine anaphase bridges, chromosome breaks and aberrations. *Nat. Cell Biol.* **20**, 92–103 (2018).
28. Chan, K. L. & Hickson, I. D. On the origins of ultra-fine anaphase bridges. *Cell Cycle* **8**, 3065–3066 (2009).
29. Hengeveld, R. C. C. et al. Rif1 is required for resolution of ultrafine DNA bridges in anaphase to ensure genomic stability. *Dev. Cell* **34**, 466–474 (2015).
30. van Mameren, J. et al. Unraveling the structure of DNA during overstretching by using multicolor, single-molecule fluorescence imaging. *Proc. Natl. Acad. Sci. USA* **106**, 18231–18236 (2009).
31. van Mameren, J. et al. Counting RAD51 proteins disassembling from nucleoprotein filaments under tension. *Nature* **457**, 745–748 (2009).
32. Farge, G. et al. Protein sliding and DNA denaturation are essential for DNA organization by human mitochondrial transcription factor A. *Nat. Commun.* **3**, 1013 (2012).
33. Brouwer, I. et al. Sliding sleeves of XRCC4–XLF bridge DNA and connect fragments of broken DNA. *Nature* **535**, 566–569 (2016).
34. Wuite, G. J., Smith, S. B., Young, M., Keller, D. & Bustamante, C. Single-molecule studies of the effect of template tension on T7 DNA polymerase activity. *Nature* **404**, 103–106 (2000).
35. Karow, J. K., Chakraverty, R. K. & Hickson, I. D. The Bloom's syndrome gene product is a 3′–5′ DNA helicase. *J. Biol. Chem.* **272**, 30611–30614 (1997).
36. Brosh, R. M. Jr. et al. Replication protein A physically interacts with the Bloom's syndrome protein and stimulates its helicase activity. *J. Biol. Chem.* **275**, 23500–23508 (2000).
37. Xue, X., Raynard, S., Busygina, V., Singh, A. K. & Sung, P. Role of replication protein A in double Holliday junction dissolution mediated by the BLM–Topo IIIα–RMI1–RMI2 protein complex. *J. Biol. Chem.* **288**, 14221–14227 (2013).
38. Stark, W. M., Sherratt, D. J. & Boocock, M. R. Site-specific recombination by Tn3 resolvase: topological changes in the forward and reverse reactions. *Cell* **58**, 779–790 (1989).
39. Harmon, F. G., Brockman, J. P. & Kowalczykowski, S. C. RecQ helicase stimulates both DNA catenation and changes in DNA topology by topoisomerase III. *J. Biol. Chem.* **278**, 42668–42678 (2003).
40. Cejka, P., Plank, J. L., Dombrowski, C. C. & Kowalczykowski, S. C. Decatenation of DNA by the *S. cerevisiae* Sgs1–Top3–Rmi1 and RPA complex: a mechanism for disentangling chromosomes. *Mol. Cell* **47**, 886–896 (2012).
41. Gaymes, T. J. et al. Increased error-prone non homologous DNA end-joining—a proposed mechanism of chromosomal instability in Bloom's syndrome. *Oncogene* **21**, 2525–2533 (2002).
42. Natsume, T., Kiyomitsu, T., Saga, Y. & Kanemaki, M. T. Rapid protein depletion in human cells by auxin-inducible degron tagging with short homology donors. *Cell Rep.* **15**, 210–218 (2016).
43. Debatisse, M., Le Tallec, B., Letessier, A., Dutrillaux, B. & Brison, O. Common fragile sites: mechanisms of instability revisited. *Trends Genet.* **28**, 22–32 (2012).
44. Suski, C. & Marians, K. J. Resolution of converging replication forks by RecQ and topoisomerase III. *Mol. Cell* **30**, 779–789 (2008).
45. Trask, D. K., DiDonato, J. A. & Muller, M. T. Rapid detection and isolation of covalent DNA/protein complexes: application to topoisomerase I and II. *EMBO J.* **3**, 671–676 (1984).
46. Kung, V. T. & Wang, J. C. Purification and characterization of an omega protein from *Micrococcus luteus*. *J. Biol. Chem.* **252**, 5398–5402 (1977).
47. Smith, S. B., Cui, Y. & Bustamante, C. Overstretching B-DNA: the elastic response of individual double-stranded and single-stranded DNA molecules. *Science* **271**, 795–799 (1996).
48. Candelli, A. et al. A toolbox for generating single-stranded DNA in optical tweezers experiments. *Biopolymers* **99**, 611–620 (2013).
49. Porter, A. C. & Farr, C. J. Topoisomerase II: untangling its contribution at the centromere. *Chromosome Res.* **12**, 569–583 (2004).
50. Strick, T. R., Croquette, V. & Bensimon, D. Single-molecule analysis of DNA uncoiling by a type II topoisomerase. *Nature* **404**, 901–904 (2000).
51. Bizard, A. H. & Hickson, I. D. The dissolution of double Holliday junctions. *Cold Spring Harb. Perspect. Biol.* **6**, a016477 (2014).

52. Krejci, L., Altmannova, V., Spirek, M. & Zhao, X. Homologous recombination and its regulation. *Nucleic Acids Res.* **40**, 5795–5818 (2012).
53. Daley, J. M., Chiba, T., Xue, X., Niu, H. & Sung, P. Multifaceted role of the Topo IIIα–RMI1–RMI2 complex and DNA2 in the BLM-dependent pathway of DNA break end resection. *Nucleic Acids Res* **42**, 11083–11091 (2014).

Acknowledgements

We thank G. King for helpful discussions, H. Mankouri for helpful comments on the manuscript, M. Nadal (Institut Jacques Monod) for the *Sulfolobus solfactarius* TopA, and M. Kanemaki (National Institute of Genetics, Japan) for development of the TopoIII protein degron system. Work in the authors' laboratories is supported by the Danish National Research Fund (DNRF115), the European Union Horizon 2020 Programme 'Chromavision' (665233), the European Research Council, the Human Frontier Science Program, the Netherlands Organization for Scientific Research (NWO; 'Catching PICH in the Act' project number 741.015.002), the French National Research Agency, and the French National Cancer Institute.

Author contributions

K.S. purified proteins and DNA substrates, designed and performed biochemical, cellular, and SM experiments, and wrote the paper. A.S.B. designed and performed SM experiments and wrote the paper. A.H.B. made DNA substrate and edited the paper. J.A.M.B. performed SM experiments and edited the paper. A.G.F.-B. purified proteins, performed biochemical experiments, and edited the paper. M.M. purified proteins and edited the paper. M.P. made cell lines, performed cellular experiments, and edited the paper. Q.Y. made cell lines and edited the paper. E.J.G.P. designed experiments and wrote the paper. G.J.L.W. initiated the project, designed experiments, and wrote the paper. I.D.H. initiated the project, designed experiments, and wrote the paper.

Competing interests

The authors declare no competing interests.

Additional information

Supplementary information is available for this paper at https://doi.org/10.1038/s41594-018-0123-8.

Reprints and permissions information is available at www.nature.com/reprints.

Correspondence and requests for materials should be addressed to G.J.L.W. or I.D.H.

Publisher's note: Springer Nature remains neutral with regard to jurisdictional claims in published maps and institutional affiliations.

Methods

Reagents. All reagents, antibodies, cell culture, DNA substrate preparation, and protein expression and purification are described in Supplementary Note 1.

Single-molecule optical tweezers experiments. The experiments were performed on a custom-built inverted microscope that combines wide-field fluorescence microscopy and dual-trap optical tweezers[26]. The flow cell consisted of a custom-made glass chip, which was modified compared to published designs (Fig. 1b). It contained six inlet channels (denoted here I–VI) and two outlet channels (E1 and E2). All eight channels were connected via tubing to valves, which could be individually opened and closed. Inlet channels were connected to separate reservoirs, which were housed in a pressure box that allowed us to control flow speed. Channels I–III contained beads (streptavidin-coated polystyrene microspheres of 4.5 µm in diameter; Spherotech), biotinylated DNA, and protein-free buffer (20 mM HEPES pH 7.5, 50 mM NaCl, 1 mM $MgCl_2$, 1 mM DTT, 0.02% Tween-20, and 0.02% casein; buffer A). Channel IV was reserved for T7 DNA polymerase (concentration 40 U/ml in 20 mM HEPES pH 7.5, 50 mM NaCl, and 10 mM $MgCl_2$). Channel V/VI contained 60 nM PICH in buffer A with or without the addition of 1 mM ATP. The remaining channel contained 30 nM BLM, 20 nM TRR, 50 nM RPA (either labeled or unlabeled) or any possible combination of the three proteins in buffer B (20 mM HEPES pH, 7.5, 100 mM NaCl, 2 mM $MgCl_2$, 1 mM DTT, 0.02% Tween-20, and 0.02% casein). The effective temperature inside the flow cell during experiments was 26 °C. Apart from PICH, which displays some force dependence[26], the binding of RPA[30] and the other two proteins (Supplementary Fig. 1j,k) is insensitive to DNA tension. For the recruitment assays, we chose a consistent force of 20–25 pN throughout the recruitment and imaging process. These conditions ensure good image quality[54] and also lead to the stabilization of PICH binding to DNA.

More details about the instrumentation, the incubation procedures and the SM data analysis are described in Supplementary Note 2.

LRI reactions. All reactions have been performed in buffer R (50 mM Tris-HCl pH 7.5, 50 mM NaCl, 5 mM $MgCl_2$, 0.1 mg/ml BSA, 1 mM DTT). After pre-heating the tubes with the enzyme mix (1 min, 37 °C), the reaction was initiated by addition of the substrate mix containing 50 pM labeled LRI and 2 mM ATP to a final volume of 10 µl, and was then incubated for a further 7 min (or the indicated times) at 37 °C. Enzyme concentrations are stated in each case in the figure legends. The reaction was stopped by the addition of STOP solution (10 mM Tris-HCl pH 7.5, 30 mM EDTA, 0.5% SDS, 0.5 mg/ml proteinase K, 8% sucrose, and a mixture of Orange G, Bromophenol Blue, and Xylene Cyanol) and the samples were further incubated for 15 min at 37 °C. The samples were denatured at 80 °C for 3 min, and then immediately cooled on ice before gel loading. Samples were separated on 1.2% agarose gels in 0.5× TBE, at 3 V/cm, for 2.5 h or 1 V/cm for 16 h in the presence or absence of 0.5 µg/ml ethidium bromide. After running, the gels were dried and analyzed by PhosphorImager.

For analysis of the covalent attachment of hTopoIIIα to the 5′ end of the products (Fig. 6a,b), the reaction was quenched by the addition of 0.7% SDS, followed by incubation at 60 °C for 30 s. After this, 60 mM KCl was added, and the mixture was vortexed and incubated on ice for 5 min, followed by centrifugation at room temperature at 2,000*g*. The pellet was resuspended in 50 mM Tris-HCl, pH 7.5, and treated with STOP without SDS at 37 °C for 15 min. The supernatant was treated with STOP solution at 37 °C for 15 min.

Single-catenane reactions. The single-catenane substrate was prepared from plasmid pMM5 using Tn3 resolvase[55] as described previously[38]. The XbaI and XhoI digests were used as markers for the circular supercoiled and linear products, respectively. The biochemical experiments were performed the same way as in the case of the LRI substrate, with the following exceptions: the substrate mix contained 15 pM single-catenane substrate and 2 mM ATP, and the reactions were incubated for 15 min (or the indicated times) at 37 °C. The samples were run on 0.8% agarose gels in the presence of 0.5 µg/ml ethidium bromide, and the gels were subjected to Southern blotting after electrophoresis, as described previously[56]. An ampicillin gene cassette was used to generate the probe for the blots, which recognizes only one of the circles of the single catenane.

Dissolution of double Holliday junctions. The double–Holliday junction substrate was created and the experiments were performed as reported previously[11,57].

Reporting Summary. Further information on research design is available in the Nature Research Reporting Summary linked to this article.

Data availability

Source data are available for Figs. 2, 5, and 6 and Supplementary Figs. 1, 3, 4, and 7–9 with the paper online.

References

54. Candelli, A., Wuite, G. J. L. & Peterman, E. J. G. Combining optical trapping, fluorescence microscopy and micro-fluidics for single molecule studies of DNA–protein interactions. *Phys. Chem. Chem. Phys.* **13**, 7263–7272 (2011).
55. Krasnow, M. A. & Cozzarelli, N. R. Site-specific relaxation and recombination by the Tn3 resolvase: recognition of the DNA path between oriented *res* sites. *Cell* **32**, 1313–1324 (1983).
56. Brown, T. Southern blotting. *Curr. Protoc. Immunol.* Chapter 10, Unit 10.6A (2001).
57. Bachrati, C. Z. & Hickson, I. D. Dissolution of double Holliday junctions by the concerted action of BLM and topoisomerase IIIα. *Methods Mol. Biol.* **582**, 91–102 (2009).

nature research

Corresponding author(s): Hickson

Reporting Summary

Nature Research wishes to improve the reproducibility of the work that we publish. This form provides structure for consistency and transparency in reporting. For further information on Nature Research policies, see Authors & Referees and the Editorial Policy Checklist.

Statistical parameters

When statistical analyses are reported, confirm that the following items are present in the relevant location (e.g. figure legend, table legend, main text, or Methods section).

n/a	Confirmed	
☐	☒	The exact sample size (*n*) for each experimental group/condition, given as a discrete number and unit of measurement
☐	☒	An indication of whether measurements were taken from distinct samples or whether the same sample was measured repeatedly
☐	☐	The statistical test(s) used AND whether they are one- or two-sided *Only common tests should be described solely by name; describe more complex techniques in the Methods section.*
☐	☐	A description of all covariates tested
☐	☐	A description of any assumptions or corrections, such as tests of normality and adjustment for multiple comparisons
☐	☐	A full description of the statistics including central tendency (e.g. means) or other basic estimates (e.g. regression coefficient) AND variation (e.g. standard deviation) or associated estimates of uncertainty (e.g. confidence intervals)
☐	☐	For null hypothesis testing, the test statistic (e.g. *F*, *t*, *r*) with confidence intervals, effect sizes, degrees of freedom and *P* value noted *Give P values as exact values whenever suitable.*
☐	☐	For Bayesian analysis, information on the choice of priors and Markov chain Monte Carlo settings
☐	☐	For hierarchical and complex designs, identification of the appropriate level for tests and full reporting of outcomes
☐	☐	Estimates of effect sizes (e.g. Cohen's *d*, Pearson's *r*), indicating how they were calculated
☐	☒	Clearly defined error bars *State explicitly what error bars represent (e.g. SD, SE, CI)*

Our web collection on statistics for biologists may be useful.

Software and code

Policy information about availability of computer code

Data collection	Cell Sense, LabVIEW,
Data analysis	Image Quant, Image J, Graphpad Prism, Origin 9.3

For manuscripts utilizing custom algorithms or software that are central to the research but not yet described in published literature, software must be made available to editors/reviewers upon request. We strongly encourage code deposition in a community repository (e.g. GitHub). See the Nature Research guidelines for submitting code & software for further information.

Data

Policy information about availability of data

All manuscripts must include a data availability statement. This statement should provide the following information, where applicable:

- Accession codes, unique identifiers, or web links for publicly available datasets
- A list of figures that have associated raw data
- A description of any restrictions on data availability

We provide source data for all quantifications. These are related to Fig. 2g, Fig. 5e, Fig. 6b-c, Supplementary Fig. 1b-e, Supplementary Fig. 3d, Supplementary Fig. 4b/d, Supplementary Fig. 7c/e, Supplementary Fig. 8d, Supplementary Fig. 9a,

Field-specific reporting

Please select the best fit for your research. If you are not sure, read the appropriate sections before making your selection.

☒ Life sciences ☐ Behavioural & social sciences ☐ Ecological, evolutionary & environmental sciences

For a reference copy of the document with all sections, see nature.com/authors/policies/ReportingSummary-flat.pdf

Life sciences study design

All studies must disclose on these points even when the disclosure is negative.

Sample size	All relevant single-molecule data were based on at least 20 independent measurements (i.e. different DNA molecules). Furthermore, the measurements comprised of at least three different sets of experiments, each conducted on a different day, with fresh buffers. Additionally, we verified that different protein batches and variants (e.g., labeled vs. non-labeled) yield reproducibly similar data. All biochemical experiments were repeated at least 3-5 times. These are typical repetition numbers for in vitro studies.
Data exclusions	We did not exclude data from our analysis.
Replication	Typically, our single molecule findings are based on at least 20 independent measurements (i.e. different DNA molecules). All biochemical experiments were repeated at least three times; in many cases more than that.
Randomization	We were conducting an in vitro study were grouping or randomization of samples were not necessary.
Blinding	We did not apply blinding upon data collection.

Reporting for specific materials, systems and methods

Materials & experimental systems

n/a	Involved in the study
☐	☒ Unique biological materials
☐	☒ Antibodies
☐	☒ Eukaryotic cell lines
☒	☐ Palaeontology
☒	☐ Animals and other organisms
☒	☐ Human research participants

Methods

n/a	Involved in the study
☒	☐ ChIP-seq
☒	☐ Flow cytometry
☒	☐ MRI-based neuroimaging

Unique biological materials

Policy information about availability of materials

Obtaining unique materials	All materials used in the study are available from us or from commercial providers.

Antibodies

Antibodies used	PICH (in-house, raised in a guinea pig and 04-1540, Millipore), BLM (ab2179, Abcam and IHIC33, raised in-house in a rabbit), RMI1 (56-8, raised in house in mice), TopoIIIα (D6 (rabbit) and IE3 (mouse), provided by Aventis Pharma), RPA (ab2175-500, Abcam, and 2267S, Cell Signaling), α-Tubulin (ab18251, Abcam), Phospho-Histone H3 (07-424, Millipore), CENPA (ab13939-50, Abcam), FANCD2 (NB100-182, Novus Biologicals). The secondary antibodies for western blotting were horseradish-peroxidase coupled IgG from Sigma (anti-mouse, A4416; -rabbit, A6667; -guinea pig, A7289), and for immunofluorescence were Alexa-fluor coupled IgG from Life Technologies (488-mouse, A1101; 488-rabbit, A1108; 488-guinea pig, 11073; 568-mouse, A110004; 568-rabbit, A11011; 555-guinea pig, A21435; 568-human, A21090; 633-mouse, A21052; 647-rabbit, A31573).
Validation	PICH in house: Nielsen, C. F. et al. PICH promotes sister chromatid disjunction and co-operates with topoisomerase II in mitosis. Nat Commun 6, doi:ARTN 896210.1038/ncomms9962 (2015). IHIC 33 and D6: Wu, L. et al. The Bloom's syndrome gene product interacts with topoisomerase III. Journal of Biological Chemistry 275, 9636-9644, doi:DOI 10.1074/jbc.275.13.9636 (2000). IE3: Chan, K. L., North, P. S. & Hickson, I. D. BLM is required for faithful chromosome segregation and its localization defines a

class of ultrafine anaphase bridges. Embo J 26, 3397-3409, doi:10.1038/sj.emboj.7601777 (2007).
Validation of the commercial antibodies are available on their website.

Eukaryotic cell lines

Policy information about cell lines

Cell line source(s)	Osteosarcoma (U2OS), colon carcinoma (HCT116) and fibrosarcoma (HT1080) are all generally available.
Authentication	Cell lines were not authenticated.
Mycoplasma contamination	All cell lines were tested negative for mycoplasma contamination.
Commonly misidentified lines (See ICLAC register)	*Name any commonly misidentified cell lines used in the study and provide a rationale for their use.*